Implementation of Variable Capacitance to Improve Efficiency for Asymmetric LCC-LCC Compensated Wireless Power Transfer Systems

Zhu, Gangwei; Dong, Jianning; Wang, Jundong; Deng, Zichen; Li, Yongpeng; Bauer, Pavol

DOI
10.1109/ECCEEurope62508.2024.10751982

Publication date
2024

Document Version
Final published version

Published in
ECCE Europe 2024 - Energy Conversion Congress and Expo Europe, Proceedings

Implementation of Variable Capacitance to Improve Efficiency for Asymmetric LCC-LCC Compensated Wireless Power Transfer Systems

1st Gangwei Zhu
Department of Electrical Engineering, Mathematics and Computer Science
Delft University of Technology
Delft, the Netherlands
G.Zhu-2@tudelft.nl

2nd Jianning Dong
Department of Electrical Engineering, Mathematics and Computer Science
Delft University of Technology
Delft, the Netherlands
J.Dong-4@tudelft.nl

3rd Jundong Wang
Department of Electrical Engineering, Mathematics and Computer Science
Delft University of Technology
Delft, the Netherlands
j.wang-16@tudelft.nl

4th Zichen Deng
Department of Electrical Engineering, Mathematics and Computer Science
Delft University of Technology
Delft, the Netherlands
z.deng-4@tudelft.nl

5th Yongpeng Li
Department of Electrical Engineering, Mathematics and Computer Science
Delft University of Technology
Delft, the Netherlands
y.li-23@tudelft.nl

6th Pavol Bauer
Department of Electrical Engineering, Mathematics and Computer Science
Delft University of Technology
Delft, the Netherlands
P.Bauer@tudelft.nl

2024 Energy Conversion Congress & Expo Europe (ECCE Europe) | 979-8-3503-6444-6/24/$31.00 ©2024 IEEE | DOI: 10.1109/ECCEEurope62508.2024.10751982

***Abstract*—This paper proposes a variable-capacitance-based control strategy to improve efficiency for asymmetric LCC-LCC compensated wireless power transfer (WPT) systems. While the existing triple-phase-shift (TPS) method can achieve power regulation and wide-range zero-voltage-switching (ZVS), it results in significantly increased reactive power under asymmetric LCC-LCC compensation topology. To this end, this paper incorporates a switch-controlled-capacitor (SCC) on the primary side. The impact of variable capacitance on the system characteristics is first investigated. Furthermore, the optimal capacitor tuning factor is derived to achieve the inverter ZVS with minimal reactive power. Through the implementation of variable capacitance, the primary inductor current is notably reduced within a wide range of power. Moreover, the turn-off currents of power switches are minimized. These factors contribute to a reduction in inductor and inverter losses, thus improving the overall efficiency. Experimental results confirm that the proposed method improves the efficiency of an asymmetric LCC-LCC compensated WPT prototype, with a maximum efficiency improvement of up to 1.8%.**

***Index Terms*—Wireless power transfer, asymmetric LCC-LCC compensation, variable capacitance, efficiency improvement**

I. Introduction

In recent years, there has been a significant surge in research efforts focused on advancing wireless power transfer (WPT) technology. The WPT technology offers safe and automatic charging, which can be applied in diverse applications, such as medical implants [1], mobile phones [2], underwater devices [3], and electric vehicles (EVs) [4].

In practical WPT systems, batteries commonly serve as the loads. Throughout the battery charging process, the equivalent load resistance of the battery undergoes substantial changes. Therefore, to effectively cope with considerable load variations in practical scenarios, it is important for the WPT systems to possess wide-range power regulation capabilities [5].

A commonly adopted approach to enable wide-range power control involves adjusting the DC input and output voltages. This can be achieved by cascading DC-DC converters either on the primary side or the secondary side within the system [6], [7]. However, the addition of extra power conversion stages results in more components and power losses [8].

To avoid introducing additional DC-DC converters, some researchers and engineers focus on implementing phase-shift-modulation (PSM) for achieving power regulation. Nevertheless, the conventional PSM strategy leads to hard switching under load changes, consequently resulting in substantial switching losses [9]. In order to achieve zero-voltage-switching (ZVS) under varying load conditions, Hu. et al. proposed a variable-frequency-based PSM strategy in [10]. This approach dynamically adjusts the inverter frequency according to the load conditions, thus enabling wide-range ZVS. However, tuning the frequency in WPT systems may lead to the bifurcation phenomenon [11], [12]. Existing variable-frequency-based methods rely on system parameter design to prevent the bifurcation. In contrast to adjusting the frequency, a triple-phase-shift (TPS) control was proposed in [13] to achieve wide ZVS in a LCC-LCC compensated WPT system. The LCC-LCC compensation network provides constant coil currents under poor coupling conditions and offers more design freedom, which is widely adopted in WPT systems [14]–[17]. In the TPS approach, the phase difference between the inverter and rectifier AC voltages is introduced as a new control variable to facilitate ZVS. It is noteworthy that the existing TPS methods mostly concentrate on the symmetrical

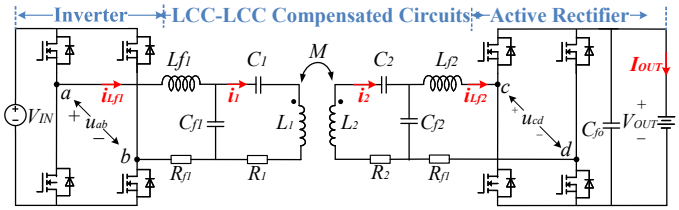

Fig. 1. Circuit diagram of the studied LCC-LCC compensated WPT system.

LCC-LCC compensation topology [13], [18]. However, in practice, the parameters of the primary and secondary sides may be asymmetrical. The parameter asymmetry can arise from two important factors [19]: firstly, variations in load voltage may lead to inconsistency between the DC input and output voltages; secondly, asymmetric coil design can result in non-symmetrical compensation parameters. In the cases of asymmetric LCC-LCC topology, the existing TPS methods lead to considerably increased reactive power in the resonant tanks, resulting in a noticeable decline in efficiency (A detailed illustration of this point of view will be shown in section II-B).

To cope with the above challenges, this paper introduces a switch-controlled-capacitor (SCC) on the primary side. Through the implementation of variable capacitance, the proposed method reduces the primary inductor current when there are parameter inconsistencies between the primary and secondary sides, thereby improving the efficiency. The main contributions of this paper are summarized as follows:

1) The asymmetric LCC-LCC compensation network is analyzed. Moreover, limitations of the existing TPS methods under asymmetric LCC-LCC compensation are demonstrated.

2) An SCC is incorporated on the primary side, and the impact of variable capacitance on the system characteristics is investigated.

3) The optimal SCC tuning factor is derived to enable the inverter ZVS with minimal reactive power. Through the implementation of optimal capacitor tuning, the proposed strategy significantly reduces the primary inductor current across a broad power range, thus reducing the inductor and inverter losses while improving the overall efficiency.

The rest of this paper is structured as follows. Section II provides an analysis of the asymmetric LCC-LCC compensation network and presents the limitations of the existing TPS methods. Subsequently, section III demonstrates the proposed method, while the experimental results are shown in section IV. Finally, section V concludes this paper.

II. Problem Formulation

A. Analysis of Asymmetric LCC-LCC Compensation

Fig. 1 demonstrates the circuit diagram of the LCC-LCC compensated WPT system. As shown in Fig. 1, the investigated system comprises three essential parts: the inverter, the active rectifier, and the LCC-LCC compensated resonant circuits. Within Fig. 1, the DC input and output voltages are V_{IN} and V_{OUT}, while the DC output current is I_{OUT}.

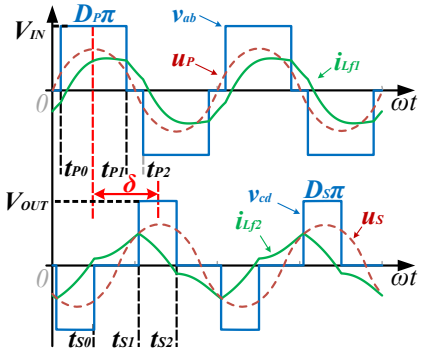

Fig. 2. Typical operating waveforms of the TPS control.

Moreover, the self-inductances of the coils are L_1 and L_2, while M indicates their mutual inductance. According to [14], the parameters of the LCC-LCC topology are configured as follows: $\omega_R L_{f1} = 1/(\omega_R C_{f1})$, $\omega_R L_{f1} = \omega_R L_1 - 1/(\omega_R C_1)$, $\omega_R L_{f2} = \omega_R L_2 - 1/(\omega_R C_2)$, $\omega_R L_{f2} = 1/(\omega_R C_{f2})$, where ω_R is the resonant frequency. Here, the subscript "1" indicates the primary side, while the subscript "2" represents the secondary side.

In the LCC-LCC compensated WPT systems, TPS control is widely employed for power regulation. Fig. 2 illustrates the operating waveforms of the existing TPS control. In Fig. 2, v_{ab} and v_{cd} are the AC voltages of the inverter and rectifier, while u_P and u_S are their fundamental components; D_P and D_S are the duty cycles of v_{ab} and v_{cd}, while δ indicates their phase difference. In the TPS control, there are three control variables: D_P, D_S, and δ. Through the control of D_P, D_S, and δ, the system is able to achieve power regulation, maximum efficiency tracking, and wide ZVS simultaneously. It is noteworthy that existing TPS methods mainly concentrate on the symmetric LCC-LCC compensation topology. However, asymmetric coils are also widely used to enhance coil misalignment tolerance and to optimize component stress [19]. The asymmetric coil design leads to asymmetric compensation parameters. Therefore, it is preferable to extend the existing analysis into the asymmetric LCC-LCC topology. In this paper, the asymmetric LCC-LCC compensation network is adopted, and the corresponding analysis is presented as follows.

(1) Power Regulation: Based on the analysis in [13] and extending it to the asymmetric LCC-LCC topology, the output power of the system is derived as

$$P_{out} = \frac{8V_{IN}V_{OUT}M}{\pi^2\omega L_{f1}L_{f2}}\sin(\frac{D_P\pi}{2})\sin(\frac{D_S\pi}{2})\sin(\delta). \quad (1)$$

As evident from (1), the output power of the system can be regulated by adjusting D_P, D_S, and δ.

(2) Maximum Efficiency Tracking: Moreover, the transmission efficiency of the asymmetric LCC-LCC compensated resonant circuits is derived as

$$\eta \approx \omega M L_{f1}L_{f2}|\sin(\delta)| \times [(R_2L_{f1}^2 + M^2R_{Lf1})T_{AC} + (R_1L_{f2}^2 + M^2R_{Lf2})/T_{AC} + \omega M L_{f1}L_{f2}|\sin(\delta)|]^{-1}, \quad (2)$$

where

$$T_{AC} = \frac{|u_S|}{|u_P|} = \frac{2\sqrt{2}\sin(D_S\pi/2)V_{OUT}/\pi}{2\sqrt{2}\sin(D_P\pi/2)V_{IN}/\pi}. \quad (3)$$

As evident in (3), T_{AC} is the AC voltage gain of the resonant circuits. Moreover, observing (2) reveals that the maximum efficiency of the resonant circuits is achieved when T_{AC} satisfies

$$T_{AC\_OPT} = \sqrt{\frac{bR_1 + cR_{Lf2}}{R_2/b + cR_{Lf1}}}, \quad (4)$$

where $b = L_{f2}/L_{f1}$, $c = M^2/(L_{f1}L_{f2})$. Further substituting (3) into (4) yields

$$\frac{\sin(D_S\pi/2)}{\sin(D_P\pi/2)} = \frac{V_{IN}}{V_{OUT}}\sqrt{\frac{bR_1 + cR_{Lf2}}{R_2/b + cR_{Lf1}}}. \quad (5)$$

To achieve maximum efficiency tracking for the resonant circuits, the inverter and rectifier duty cycles D_P and D_S should satisfy (5).

(3) ZVS Implementation: In the TPS control, achieving ZVS can be accomplished by adjusting the phase difference angle δ. For analytical convenience, the value of δ is represented as $\delta = \pi/2 + \Delta\delta$, where $\Delta\delta$ denotes the compensation phase angle. As the value of $\Delta\delta$ increases, the deviation between δ and $\pi/2$ increases accordingly, leading to elevated reactive power while facilitating ZVS. In the asymmetric LCC-LCC topology, to realize the inverter ZVS with minimal reactive power, $\Delta\delta$ needs to be configured as

$$\Delta\delta_1 = \cos^{-1}\{\frac{1}{8MV_2\sin(D_S\pi/2)} \times [-2\pi\omega L_{f1}L_{f2}I_{ZVS} + V_1L_{f2}(D_P\pi^2 - 8\sin^2(D_P\pi/2))]\} - D_P\pi/2, \quad (6)$$

Similarly, to achieve the rectifier ZVS with minimal reactive power, $\Delta\delta$ should be designed as

$$\Delta\delta_2 = \cos^{-1}\{\frac{1}{8MV_1\sin(D_P\pi/2)} \times [-2\pi\omega L_{f1}L_{f2}I_{ZVS} + V_2L_{f1}(D_S\pi^2 - 8\sin^2(D_S\pi/2))]\} - D_S\pi/2. \quad (7)$$

Finally, in order to achieve ZVS for both the inverter and rectifier, $\Delta\delta$ is set as

$$\Delta\delta = \max(\Delta\delta_1, \Delta\delta_2). \quad (8)$$

B. Limitations of Existing TPS Control

Based on the above analysis, the existing TPS control exhibits a limitation when the primary and secondary parameters are not symmetric. As evident from (5), (6) and (7), when the dual-side parameters are not symmetric, there is a gap between $\Delta\delta_1$ and $\Delta\delta_2$. With the parameters listed in Table. I, Fig. 3 demonstrates the disparity between $\Delta\delta_1$ and $\Delta\delta_2$ under different output power and voltages. As illustrated in Fig. 3, the disparity between $\Delta\delta_1$ and $\Delta\delta_2$ becomes significant with varying output power and voltages. Nevertheless, in the existing TPS control, $\Delta\delta$ is configured as the maximum value of $\Delta\delta_1$ and $\Delta\delta_2$ to ensure ZVS for both the inverter and rectifier. The gap between $\Delta\delta_1$ and $\Delta\delta_2$ results in extra reactive power. Take the case of $V_{OUT} = 450\ V$ as an example, although the inverter ZVS can be achieved with $\Delta\delta_1$, $\Delta\delta$ must be chosen as $\Delta\delta_2$ to ensure the rectifier ZVS. Since $\Delta\delta_2$ is significantly larger than $\Delta\delta_1$ in most power ranges at $V_{OUT} = 450\ V$, the existing TPS control leads to a noticeable surplus of reactive power on the primary side.

TABLE I
SYSTEM CONFIGURATIONS OF THE STUDIED ASYMMETRIC LCC-LCC COMPENSATED SYSTEM

Symbol	Parameters	Value	Unit
M	Mutual inductance	95.0	μH
L_1, L_2	Coil inductances	335.8, 224.7	μH
C_1, C_2	Series capacitances	14.8, 25.3	nF
C_{f1}, C_{f2}	Parallel capacitances	33.1, 41.3	nF
L_{f1}, L_{f2}	Compensation inductances	103.8, 83.8	μH
R_1, R_2	Coil resistances	0.45, 0.30	Ω
R_{Lf1}, R_{Lf2}	Inductor resistances	0.20, 0.14	Ω
V_{IN}	DC input voltage	300	V
V_{OUT}	DC output voltage	450	V
f_s	Resonant frequency	85	kHz

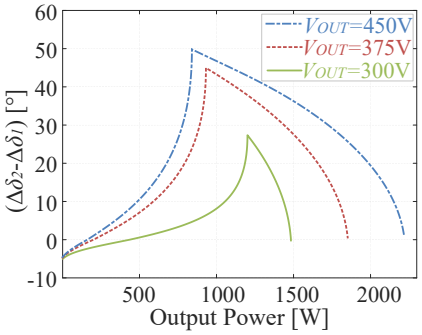

Fig. 3. Disparity between $\Delta\delta_2$ and $\Delta\delta_1$ in various output power and voltages.

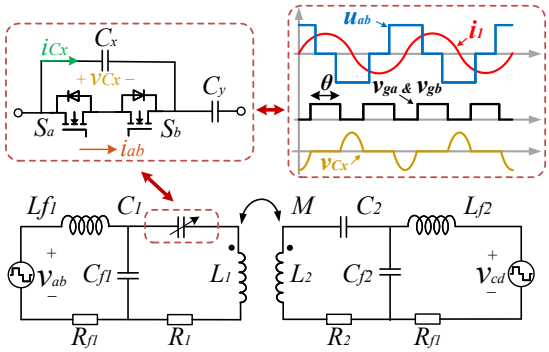

Fig. 4. Circuit topology and operating waveforms of the utilized SCC.

III. IMPLEMENTATION OF VARIABLE CAPACITANCE

A. Impact of Variable Capacitance

To address the above-mentioned additional reactive power, a primary-side SCC is implemented to replace the compensation capacitor C_1. Fig. 4 demonstrates the circuit topology and operating waveforms of the utilized SCC. As shown in Fig. 4, the SCC equivalent capacitance can be regulated by adjusting

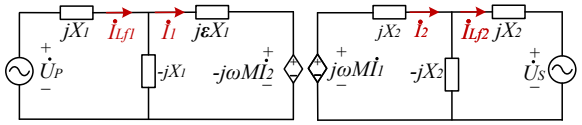

Fig. 5. Simplified equivalent model of the proposed WPT system.

the conduction angle θ. Based on the analysis in [20], the SCC equivalent capacitance is given by

$$C_{1\_eq} = \frac{\pi C_x C_y}{\pi C_x + \pi C_y - \theta C_y + \sin(\theta) C_y}. \tag{9}$$

Furthermore, to analyze the impact of variable capacitance, the capacitor tuning coefficient ε is specified as

$$\varepsilon = \frac{\omega L_1 - 1/(\omega C_{1\_eq})}{X_1}, \tag{10}$$

where $X_1 = \omega L_{f1}$ indicates the primary characteristic reactance. As it can be observed from (9) and (10), adjusting the SCC equivalent capacitance allows for the corresponding regulation of ε. In the rest of this paper, the term ε will be employed to indicate the SCC tuning degree for simplicity. With the definition of ε, the simplified equivalent model of the proposed system is shown in Fig. 5. Here, $X_2 = \omega L_{f2}$ is the secondary characteristic reactance. Moreover, by applying Kirchhoff's Voltage Law (KVL) to this model, the impact of variable capacitance is illustrated as follows.

(1) Impact on Coil Currents: The coil currents $\dot{I}_1$ and $\dot{I}_2$ are derived as

$$\dot{I}_1 = -j\frac{\dot{U}_P}{X_1}, \dot{I}_2 = j\frac{\dot{U}_S}{X_2}. \tag{11}$$

As evident from (11), the SCC tuning coefficient ε is absent in the expressions of $\dot{I}_1$ and $\dot{I}_2$, indicating that SCC tuning does not impact the coil currents.

(2) Impact on Inductor Currents: Moreover, the inductor currents $\dot{I}_{Lf1}$ and $\dot{I}_{Lf2}$ are derived as

$$\dot{I}_{Lf2} = -j\frac{\omega M}{X_1 X_2}\dot{U}_P, \tag{12}$$

$$\dot{I}_{Lf1} = j\frac{\varepsilon - 1}{X_1}\dot{U}_P + j\frac{\omega M}{X_1 X_2}\dot{U}_S. \tag{13}$$

Observing (12) reveals that the SCC tuning does not influence $\dot{I}_{Lf2}$. However, further examination of (13) indicates that both the amplitudes and phase angles of $\dot{I}_{Lf1}$ can be adjusted through SCC tuning. This introduces a new control variable for achieving inverter ZVS by dynamically regulating $\dot{I}_{Lf1}$. Details on how to design the optimal SCC tuning factor ε to minimize $\dot{I}_{Lf1}$ will be discussed in section III-B.

(3) Impact on Power Delivery: The output power of the proposed system is derived as

$$P_{out} = \mathrm{Re}\{\dot{U}_S \dot{I}^*_{Lf2}\} = \frac{M}{\omega L_{f1} L_{f2}}|\dot{U}_P||\dot{U}_S|\sin(\delta) \tag{14}$$

As shown in (14), the output power is determined by the AC voltages of the inverter and rectifier, while tuning the SCC does not influence the power delivery.

B. Optimal SCC Tuning Coefficient for Inverter ZVS

According to [13], to realize the inverter ZVS with minimal reactive power, the following criteria need to be satisfied:

$$i_{Lf1}(t_{P0}) = -I_{ZVS}, \tag{15}$$

where I_{ZVS} is the threshold current for charging/discharging the equivalent output capacitance C_{oss} of the power switches. To investigate the optimal ZVS condition shown in (15), it is necessary to derive the time-domain expression of i_{Lf1}. Based on [13], it is important to consider the high-order harmonics in $i_{Lf1}(t)$ for ZVS analysis. The harmonic-considered ZVS analysis is illustrated as follows.

Firstly, owing to the filtering effects of L_{f1} and C_{f1}, the voltage across C_{f1} (designated as u_{Cf1}) exhibits little high-order harmonics. Therefore, the expression of $u_{Cf1}(t)$ can still be derived based on the FHA method. The time-domain expression of $u_{Cf1}(t)$ is given by

$$\begin{aligned} u_{Cf1}(t) \quad &= \frac{4\varepsilon V_1}{\pi}\sin(\frac{D_P\pi}{2})\sin(\omega t) + \frac{4MV_2}{\pi L_{f2}}\sin(\frac{D_S\pi}{2}) \\ &\times\sin(\omega t - \pi/2 - \Delta\delta), \end{aligned} \tag{16}$$

Secondly, by applying KVL to the circuit diagram shown in Fig. 4, the following differential equation is obtained as

$$v_{ab}(t) - u_{Cf1}(t) = L_{f1}\frac{di_{Lf1}(t)}{dt}. \tag{17}$$

As illustrated in Fig. 2, the inverter output voltage v_{ab} remains at V_{IN} during the time interval of $t_{P0} < t < t_{P1}$. In this interval, the time-domain expression of $i_{Lf1}(t)$ is given by

$$i_{Lf1}(t) = i_{Lf1}(t_{P0}) + \frac{1}{L_{f1}}\int_{t_{P0}}^{t}[V_{IN} - u_{Cf1}(\tau)]d\tau. \tag{18}$$

Furthermore, v_{ab} remains at 0 during the period of $t_{P1} < t < t_{P2}$. Within this period, the time-domain expression of $i_{Lf1}(t)$ is represented by

$$i_{Lf1}(t) = i_{Lf1}(t_{P1}) + \frac{1}{L_{f1}}\int_{t_{P1}}^{t}[-u_{Cf1}(\tau)]d\tau. \tag{19}$$

Thirdly, considering the symmetrical characteristics of the current waveforms, it is evident that

$$i_{Lf1}(t_{P0}) = -i_{Lf1}(t_{P2}). \tag{20}$$

Combining (16), (18), (19), and (20), the value of $i_{Lf1}(t_{P0})$ is derived as

$$\begin{aligned} i_{Lf1}(t_{P0}) = \quad &-\frac{V_1 D_P\pi}{2\omega L_{f1}} + \frac{4\varepsilon V_1}{\pi\omega L_{f1}}\sin^2(\frac{D_P\pi}{2}) \\ &+\frac{4MV_2}{\pi\omega L_{f1}L_{f2}}\sin(\frac{D_S\pi}{2})\cos(\frac{D_P\pi}{2} + \Delta\delta). \end{aligned} \tag{21}$$

Finally, substituting (15) into (21) obtains the optimal SCC tuning coefficient for the inverter ZVS, which is given by

$$\begin{aligned} \varepsilon_{opt} = \quad &\Gamma^{-1} \times [-2\pi\omega L_{f1}L_{f2}I_{ZVS} + V_1 L_{f2} D_P\pi^2 \\ &-8MV_2\sin(D_S\pi/2)\cos(D_P\pi/2 + \Delta\delta)], \end{aligned} \tag{22}$$

where $\Gamma = 8V_1 L_{f2}\sin^2(D_P\pi/2)$.

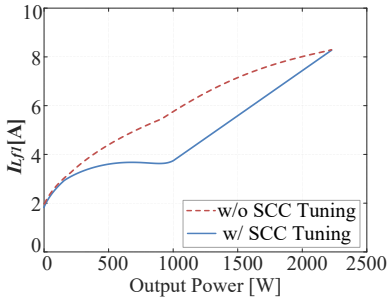

Fig. 6. The RMS value of the primary inductor current with and without SCC tuning.

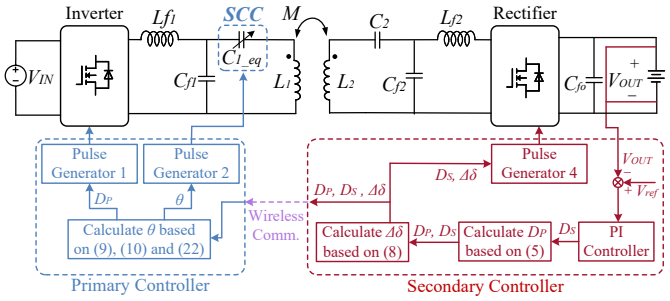

Fig. 7. Block diagram of the proposed control strategy.

According to the above analysis, it is apparent that by adjusting the SCC coefficient ε to ε_{opt}, the inverter ZVS can be realized with minimal reactive power.

It is noteworthy that in this paper, achieving rectifier ZVS is still accomplished by adjusting the compensation phase angle $\Delta\delta$ as outlined in (8). The proposed method aims to incorporate the SCC to mitigate excess reactive power on the primary side, thus reducing the primary inductor current while improving efficiency.

C. Reduction of Primary Inductor Current

To validate the effectiveness of variable capacitance, Fig. 6 illustrates the calculated RMS value of the primary inductor current with and without SCC tuning. Notably, as previously discussed in section III-A, the SCC tuning does not impact the coil currents, the secondary inductor current, and the output power. However, the primary inductor current i_{Lf1} can be adjusted. As shown in Fig. 6, the introduction of SCC tuning leads to a notable reduction in I_{Lf1} across wide power ranges. This reduction not only diminishes power losses in the primary inductor L_{f1} but also lowers conduction and turn-off losses for the inverter, thereby enhancing the efficiency of the system.

D. Control Block Diagram

Fig. 7 demonstrates the block diagram of the proposed control strategy. The DC output voltage is initially measured. A PI controller is then employed for voltage tracking, generating the rectifier duty cycle D_S. Afterward, the inverter duty cycle D_P is calculated using (5). After obtaining the values of D_P and D_S, the compensation angle $\Delta\delta$ is computed using (8) to implement ZVS. Moreover, the SCC control angle θ is derived through (9), (10), and (22). This SCC control angle is then applied to the primary-side SCC. The SCC tuning decreases the primary-side reactive power, thereby reducing the primary inductor current and enhancing efficiency.

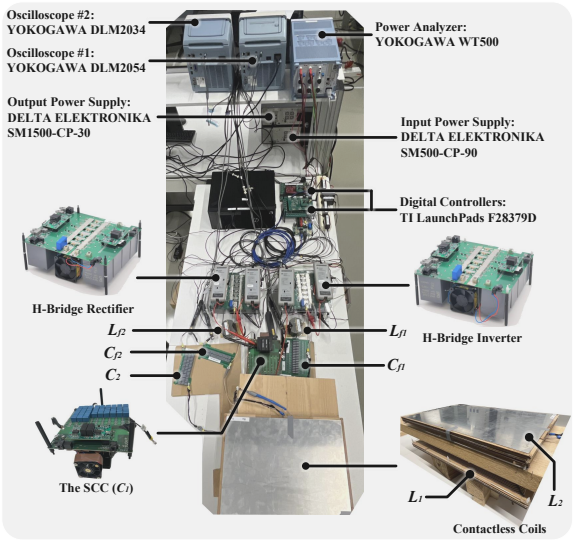

Fig. 8. Asymmetric LCC-LCC compensated WPT prototype.

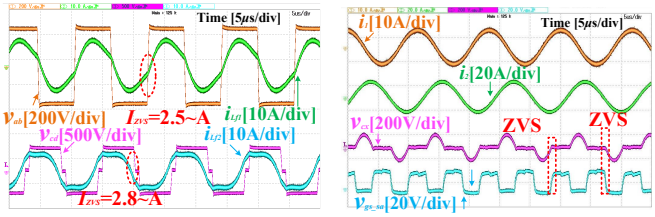

(a) (b)

Fig. 9. Steady-state waveforms of the proposed method when transferring 1.8 kW power: (a) operating waveforms of v_{ab}, v_{cd}, i_{Lf1}, and i_{Lf2}; (b) operating waveforms of i_1, i_2, v_{cx}, and v_{gs_sa}.

IV. Experimental Results

To validate the proposed approach, experiments were conducted using an asymmetric LCC-LCC compensated WPT prototype, as depicted in Fig. 8. In this setup, two H-bridge converters are adopted as the inverter and rectifier, while a primary-side SCC is assembled to allow for variable capacitance. The system is powered by a DC source, with the DC input voltage configured as 300 V, while another bidirectional DC source was employed to function as the load. The algorithm and pulse generation of the proposed control technique were implemented in TI Launchpads F28379D. To implement ZVS for the power switches, the threshold ZVS current was set to 2 A. More detailed parameters of the prototype can be found in Table. I.

Fig. 9 shows the steady-state waveforms of the proposed approach when transferring 1.8 kW power. As shown in Fig. 9(a), the proposed strategy implements ZVS for both the

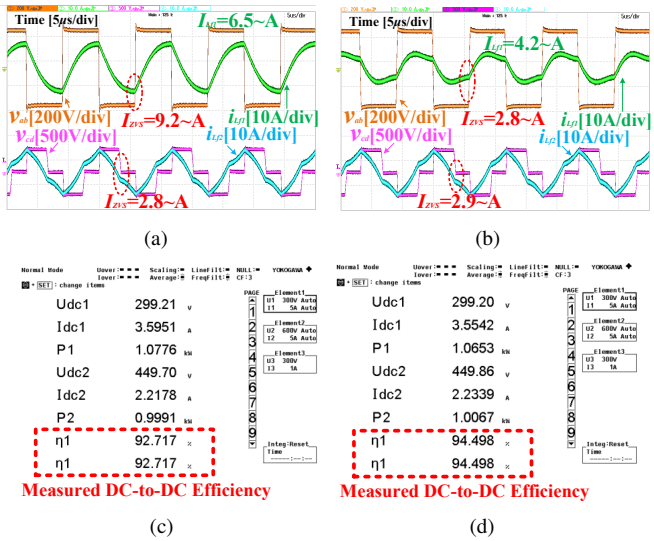

Fig. 10. Comparisons between the proposed method and the existing TPS method when transferring 1.0 kW power: operating waveforms of (a) the existing TPS control, and (b) the proposed method; measured DC-to-DC efficiency of (c) the existing TPS control, and (d) the proposed method.

inverter and rectifier, and the minimum ZVS currents are both regulated around the designed value. On the other hand, as evident from Fig. 9(b), the SCC achieves ZVS as well. As a result, the switching losses of the SCC MOSFETs are minimized.

Fig. 10 provides a comparative analysis of the proposed method and the existing TPS method when transferring 1.0 kW power. As illustrated in Fig. 10(a), the RMS value of i_{Lf1} is 6.5 A in the TPS control, while the minimum ZVS current of the inverter is 9.2 A. Nevertheless, owing to the implementation of variable capacitance, as depicted in Fig. 10(b), I_{Lf1} is reduced from 6.5 A to 4.2 A in the proposed method, and the minimum ZVS current of the inverter is decreased from 9.2 A to 2.8 A. The reduced primary inductor current contributes to less inductor and inverter losses. As shown in Fig. 10(c) and 10(d), when compared with the existing TPS method, the measured DC-to-DC efficiency is improved from 92.7 % to 94.5 % in the proposed approach.

Fig. 11 further compares the measured efficiency of the proposed method and the existing TPS method at various output power levels. Experimental results demonstrate that the proposed method improves the efficiency across a wide power range, achieving a maximum improvement of 1.8 %.

V. Conclusions

In this paper, a primary-side SCC is implemented to enhance efficiency for asymmetric LCC-LCC compensated WPT systems. Based on the analysis of the asymmetric LCC-LCC network, this paper demonstrates that the existing TPS method leads to extra reactive power when there are parameter inconsistencies between the primary and secondary sides. A variable-capacitance-based control technique is then proposed to deal with the above limitations. The impact of variable

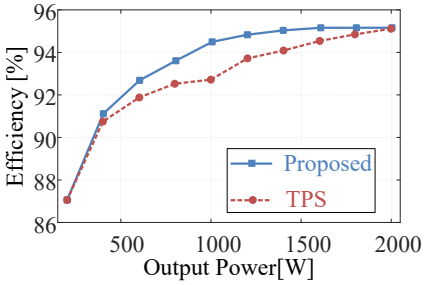

Fig. 11. Measured DC-to-DC efficiency of the proposed method and the existing TPS method at various output power levels.

capacitance on the system characteristics is investigated. Moreover, an optimal capacitor tuning strategy is proposed to minimize the reactive power. Experimental results show that the proposed method reduces the primary inductor current across a wide power range, thus improving the system's efficiency.

References

[1] X. Cao, H. Sato, K.-D. Xu, W. Jiang, S. Gong, and Q. Chen, "A systematic method for efficient wireless powering to implantable biomedical devices," *IEEE Transactions on Antennas and Propagation*, vol. 71, no. 3, pp. 2745–2757, 2023.

[2] Y. Wang, Z. Sun, Y. Guan, and D. Xu, "Overview of megahertz wireless power transfer," *Proceedings of the IEEE*, 2023.

[3] F. Chen, J. Zhang, S. Cui, Z. Bie, C. Zhu *et al.*, "A novel pendulum-type magnetic coupler with high misalignment tolerance for auv underwater wireless power transfer systems," *IEEE Transactions on Power Electronics*, 2023.

[4] Z. Deng, H. Hu, Y. Su, F. Chen, J. Xiao, C. Tang, and T. Lin, "Design of a 60kw ev dynamic wireless power transfer system with dual transmitters and dual receivers," *IEEE Journal of Emerging and Selected Topics in Power Electronics*, 2023.

[5] G. Zhu, J. Dong, W. Shi, T. B. Soeiro, J. Xu, and P. Bauer, "A mode-switching-based phase shift control for optimized efficiency and wide zvs operations in wireless power transfer systems," *IEEE Transactions on Power Electronics*, vol. 38, no. 4, pp. 5561–5575, 2022.

[6] M. Gheisarnejad, H. Farsizadeh, M.-R. Tavana, and M. H. Khooban, "A novel deep learning controller for dc–dc buck–boost converters in wireless power transfer feeding cpls," *IEEE Transactions on Industrial Electronics*, vol. 68, no. 7, pp. 6379–6384, 2020.

[7] G. Yu, J. Dong, T. B. Soeiro, G. Zhu, Y. Yao, and P. Bauer, "Three-mode variable-frequency zvs modulation for four-switch buck+ boost converters with ultra-high efficiency," *IEEE Transactions on Power Electronics*, vol. 38, no. 4, pp. 4805–4819, 2022.

[8] I.-W. Iam, C.-K. Choi, C.-S. Lam, P.-I. Mak, and R. P. Martins, "A constant-power and optimal-transfer-efficiency wireless inductive power transfer converter for battery charger," *IEEE Transactions on Industrial Electronics*, 2023.

[9] Y. Li, J. Hu, F. Chen, Z. Li, Z. He, and R. Mai, "Dual-phase-shift control scheme with current-stress and efficiency optimization for wireless power transfer systems," *IEEE Transactions on Circuits and Systems I: Regular Papers*, vol. 65, no. 9, pp. 3110–3121, 2018.

[10] H. Hu, T. Cai, S. Duan, X. Zhang, J. Niu, and H. Feng, "An optimal variable frequency phase shift control strategy for zvs operation within wide power range in ipt systems," *IEEE Transactions on Power Electronics*, vol. 35, no. 5, pp. 5517–5530, 2019.

[11] G. Zhu, J. Dong, F. Grazian, and P. Bauer, "A parameter recognition based impedance tuning method for ss-compensated wireless power transfer systems," *IEEE Transactions on Power Electronics*, 2023.

[12] G. Zhu, J. Dong, and P. Bauer, "A dynamic frequency sweeping based parameter estimation method for wireless power transfer," in *IECON 2023-49th Annual Conference of the IEEE Industrial Electronics Society*. IEEE, 2023, pp. 1–6.

[13] X. Zhang, T. Cai, S. Duan, H. Feng, H. Hu, J. Niu, and C. Chen, "A control strategy for efficiency optimization and wide zvs operation range in bidirectional inductive power transfer system," *IEEE Transactions on Industrial Electronics*, vol. 66, no. 8, pp. 5958–5969, 2018.
[14] S. Li, W. Li, J. Deng, T. D. Nguyen, and C. C. Mi, "A double-sided lcc compensation network and its tuning method for wireless power transfer," *IEEE transactions on Vehicular Technology*, vol. 64, no. 6, pp. 2261–2273, 2014.
[15] J. Li, X. Zhang, and X. Tong, "Research and design of misalignment-tolerant lcc–lcc compensated ipt system with constant-current and constant-voltage output," *IEEE Transactions on Power Electronics*, vol. 38, no. 1, pp. 1301–1313, 2022.
[16] G. Zhu, J. Dong, G. Yu, W. Shi, C. Riekerk, and P. Bauer, "Optimal multivariable control for wide output regulation and full-range efficiency optimization in lcc-lcc compensated wireless power transfer systems," *IEEE Transactions on Power Electronics*, pp. 1–14, 2024.
[17] C. Cheng, F. Lu, Z. Zhou, W. Li, Z. Deng, F. Li, and C. Mi, "A load-independent lcc-compensated wireless power transfer system for multiple loads with a compact coupler design," *IEEE Transactions on Industrial Electronics*, vol. 67, no. 6, pp. 4507–4515, 2019.
[18] N. Fu, J. Deng, Z. Wang, and D. Chen, "An lcc–lcc compensated wpt system with switch-controlled capacitor for improving efficiency at wide output voltages," *IEEE Transactions on Power Electronics*, 2023.
[19] S. Ann and B. K. Lee, "Analysis of impedance tuning control and synchronous switching technique for a semibridgeless active rectifier in inductive power transfer systems for electric vehicles," *IEEE Transactions on Power Electronics*, vol. 36, no. 8, pp. 8786–8798, 2021.
[20] X. Wang, J. Xu, M. Leng, H. Ma, and S. He, "A hybrid control strategy of lcc-s compensated wpt system for wide output voltage and zvs range with minimized reactive current," *IEEE Transactions on Industrial Electronics*, vol. 68, no. 9, pp. 7908–7920, 2020.